Journal of Alloys and Compounds 613 (2014) 338–343

Contents lists available at ScienceDirect

Journal of Alloys and Compounds

journal homepage: www.elsevier.com/locate/jalcom

Improved persistent luminescence of $CaTiO_3$:Pr by fluorine substitution and thermochemical treatment

Songhak Yoon [a,*], Eugenio H. Otal [a], Alexandra E. Maegli [a], Lassi Karvonen [a], Santhosh K. Matam [a], Stefan G. Ebbinghaus [b], Bernhard Walfort [c], Hans Hagemann [d], Simone Pokrant [a], Anke Weidenkaff [a,e]

[a] Laboratory for Solid State Chemistry and Catalysis, Empa – Swiss Federal Laboratories for Materials Science and Technology, Überlandstrasse 129, CH-8600 Dübendorf, Switzerland
[b] Institute of Chemistry, Martin-Luther-University Halle-Wittenberg, Kurt-Mothes-Strasse 2, 06120 Halle/Saale, Germany
[c] LumiNova AG, Speicherstrasse 60A, CH-9053 Teufen, Switzerland
[d] Department of Physical Chemistry, University of Geneva, Quai E. Ansermet 30, CH-1211 Geneva 4, Switzerland
[e] Institute for Materials Science, University of Stuttgart, Heisenbergstrasse 3, 70569 Stuttgart, Germany

ARTICLE INFO

Article history:
Received 26 March 2014
Received in revised form 6 June 2014
Accepted 6 June 2014
Available online 17 June 2014

Keywords:
$CaTiO_3$:Pr
Fluorination
Persistent luminescence
Afterglow
X-ray diffraction

ABSTRACT

Fluorine-substituted $CaTiO_3$:Pr phosphors were prepared by a solid-state reaction. Rietveld refinements of powder X-ray diffraction patterns revealed that increasing fluorine-substitution leads to the gradual shrinkage of the unit-cell. Enhanced afterglow intensities were observed with fluorine-substitution. Furthermore, the effect of annealing atmosphere was investigated by thermochemical treatment in different atmospheres (Ar, air and NH_3). UV–Vis diffuse reflectance spectra and photoluminescence excitation spectra revealed that Pr^{4+} in the pristine $CaTi(O,F)_3$:Pr phosphor was partially reduced to Pr^{3+} under NH_3 flow leading to an intensity improvement of ca. 450% compared to $CaTiO_3$:Pr. The substantial improvement of afterglow intensity by fluorine substitution and annealing in NH_3 is considered to be connected with the generation of oxygen vacancies and the partial reduction of Pr^{4+} to Pr^{3+}.

1. Introduction

Strong red phosphorescence of $CaTiO_3$:Pr has been widely stzudied during the last decades because of the potential application in phosphor lamps, soft illumination, warning signs or field emission displays [1–5]. The persistent luminescence was attributed to detrapping of electrons stored in trapping centers like oxygen vacancies by thermal activation, followed by red emission due to the $^1D_2 \rightarrow {}^3H_4$ transition of Pr^{3+} [1,2].

Many attempts have been devoted to the improvement of the emission intensity and to the enhancement of the phosphorescence efficiency, and various factors affecting the phosphorescence have been discussed. It is well accepted that the concentration of oxygen vacancies is a decisive factor to explain the phosphorescence behavior of $CaTiO_3$:Pr [3,4]. With respect to these findings different methodologies, for example, synthesis method variation, different co-substitutions and host modifications have been pursued [3,5–10]. For example, in addition to Al^{3+}, Bi^{3+} and In^{3+} [6–8], Zn^{2+} and/or B^{3+} substitution [9,10] have been found to intensify the red emission of $CaTiO_3$:Pr^{3+}. Adding 3% Ca excess followed by thermal treatment at 1400 °C resulted in significant afterglow improvement [11]. On the other hand, comparatively few studies have been carried out concerning the anionic substitution and the influence of annealing atmosphere on persistent luminescence.

In the present study, $CaTi(O,F)_3$:Pr powders were synthesized by a solid-state reaction. Because of the different formal charges and ionic radii of O^{2-} and F^-, the distribution and concentration of the defects (including oxygen vacancies) can be varied depending on the degree of fluorine-substitution in $CaTiO_3$:Pr. A partial substitution of oxygen with fluorine can change the oxidation state of titanium and/or praseodymium, which can subsequently alter the luminescence properties of the oxyfluorides in comparison with the oxides. Furthermore, the luminescence properties can also be influenced by the choice of annealing conditions, which affects the concentration of oxygen vacancies and the oxidation state of praseodymium. The influence of annealing atmosphere with varied fluorine content is systematically investigated and the resulting afterglow decay behavior is studied by fluorescence spectrophotometry.

2. Experimental procedures

$CaTiO_3$:Pr^{3+} powder was synthesized by a solid-state reaction. 0.1 mol of $CaCO_3$ (Merck, 99.5%) and 0.1 mol of TiO_2 (Sigma–Aldrich, ⩾98.5%) together with 2 mmol of Pr_2O_3 (Alfa Aesar, 99.9%) were thoroughly mixed using agate mortar and pestle. The powder mixtures were calcined first at 700 °C for 12 h. After an intermediate grinding step, the powders were heated at 1100 °C for 12 h in air twice with another

* Corresponding author.
E-mail address: songhak.yoon@empa.ch (S. Yoon).

http://dx.doi.org/10.1016/j.jallcom.2014.06.041
0925-8388/

intermediate grinding in order to achieve phase purity. Both heating and cooling rates were set to 5 °C/min. The obtained $CaTiO_3:Pr^{3+}$ powder is denoted in the following as CTO. For the substitution of O^{2-} by F^-, CaF_2 (Sigma Aldrich, ⩾98.5%) was used. The same procedure of heat treatment as above was applied for the substitution series. Stoichiometric amounts of CaF_2, $CaCO_3$, and TiO_2 along with Pr_2O_3 were used for the synthesis of five different phosphor powders. Details are listed in Table 1. Moreover, CTOF1.5 was selected as an example to investigate the influence of annealing atmosphere. Aliquots of the as-synthesized CTOF1.5 powder were annealed in different atmospheres, namely synthetic air, argon, and NH_3 (denoted as Ar-CTOF1.5, Air-CTOF1.5 and NH_3-CTOF1.5, respectively). For Air-CTOF1.5, 3 g of the white CTOF1.5 powder was heated (5 °C/min) to 1000 °C in a synthetic air stream (100 mL/min) and kept at this temperature for 12 h. Subsequently, the sample was cooled down with a cooling rate of 5 °C/min to room temperature. For Ar-CTOF1.5, the same annealing condition was applied with Ar atmosphere. An annealing treatment at 400 °C for 2.5 h under NH_3 flow as described in the previous paper [12] was chosen for NH_3-CTOF1.5.

Powder X-ray diffraction patterns were obtained using a PANalytical X'Pert PRO θ–2θ system equipped with a Johansson monochromator (Cu $K\alpha_1$ radiation, 1.5406 Å) and an X'Celerator linear detector. The diffraction patterns were recorded between 20° and 100° (2θ) with an angular step interval of 0.0167°. The Thompson-Cox-Hastings pseudo-Voigt function was used as profile function [13] and CeO_2 (NIST SRM674b) was measured as standard reference material in order to estimate the instrument-specific contribution to the peak broadening.

Raman spectra were recorded on a Renishaw 2000 spectrometer equipped with holographic notch filters and a CCD array detector. The samples were excited with a red He–Ne laser (632.816 nm) beam which was focused onto the sample using objective lenses (20× magnification). The instrument was calibrated with a Si single crystal. The spectra were recorded at room temperature with an exposure time of 10 s, repeated five times and accumulated.

Thermogravimetric analysis (TGA) was carried out using a NETZSCH STA 409 CD thermobalance. A baseline was initially measured with an empty alumina crucible. In each measurement around 0.1 g of sample powder was heated under synthetic air (50 mL/min) up to 1500 °C with a heating rate of 10 °C/min. Gas analysis was done with a connected quadrupole mass spectrometer (MS, NETZSCH QMS 403 C).

UV–Visible diffuse reflectance spectra were acquired using a UV-3600 Shimadzu UV–Vis NIR spectrophotometer equipped with an integrating sphere. The baseline measurement was taken with $BaSO_4$. The spectra were recorded in the range of 200–800 nm with a step interval of 2 nm.

The Photoluminescence excitation and emission spectra were obtained at room temperature using a spectrofluorometer (Fluorolog 3–22 Jobin Yvon, Edison) with a nominal resolution ranging from 0.5 to 2.0 nm.

Phosphorescence decay profiles were measured with a photometer (Phototec, RC Tritec in collaboration with Monyco) equipped with a high-sensitive photomultiplier from Hamamatsu. The spectra were recorded at room temperature after excitation by 6 UV–LED (254 nm) for one minute to fully activate the phosphors. The measurement was started 20 s after the end of the excitation.

Table 1
Detailed experimental conditions of the used precursors for the synthesis of five different $CaTi(O,F)_3:Pr^{3+}$ powders.

Sample	CTO	CTOF0.5	CTOF1.0	CTOF1.5	CTOF2.0
CaF_2 (mol)	0	0.025	0.05	0.075	0.1
$CaCO_3$ (mol)	0.1	0.075	0.05	0.025	0
TiO_2 (mol)	0.1	0.1	0.1	0.1	0.1
Pr_2O_3 (mol)	0.002	0.002	0.002	0.002	0.002

3. Results and discussion

X-ray diffraction patterns of CTO, CTOF0.5, CTOF1.0, CTOF1.5 and CTOF2.0 powders are shown in Fig. 1. All observed reflections can be assigned to the orthorhombic perovskite $CaTiO_3$ (JCPDS-PDF No. 01-082-0228). For CTOF1.0, CTOF1.5 and CTOF2.0 powders, however, traces of remaining CaF_2 (JCPDS-PDF No. 01-077-2095) and TiO_2 (JCPDS-PDF No. 01-073-2224) were detected as shown in Fig. 1(b). Quantitative phase analysis using the Rietveld method [14] revealed that 1.9 mol% of CaF_2 and 1.9 mol% of TiO_2 remained for CTOF1.5. For CTOF2.0, the remaining CaF_2 and TiO_2 phases increased to 7.0 mol% and 8.3 mol%, respectively. Fig. 2 presents the XRD pattern of CTOF1.5 with the corresponding Rietveld refinement. The refinement result for the cell parameters and unit-cell volume together with the reliability factors and goodness-of-fit indices are listed in Table 2. The unit-cell volume decreases with increasing CaF_2 content, except CTOF1.0. As the ionic radius of the fluorine ion is smaller than that of the oxygen ion ($r(F^{1-}) = 1.33$ Å and $r(O^{2-}) = 1.40$ Å [15]), the substitution of oxygen by fluorine is expected to lead to a shrinkage of the lattice. This provides indirect evidence that the incorporated fluorine content in the perovskite structure is increasing when higher contents of CaF_2 are used. However, the possible presence of oxygen

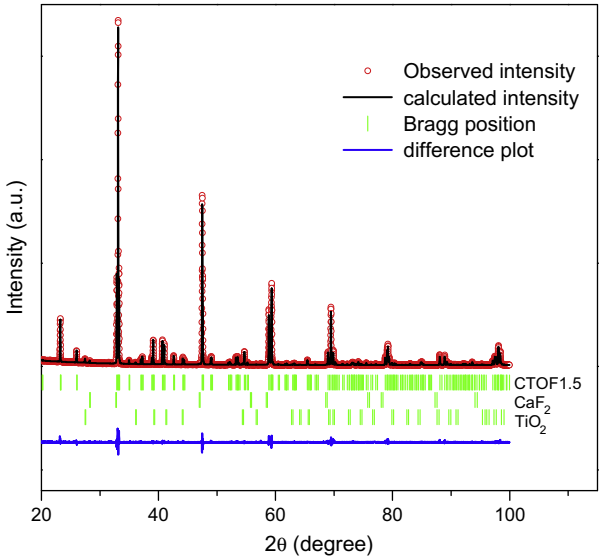

Fig. 2. Rietveld refinement plot of CTOF1.5. The difference plot of the observed and calculated diffraction profiles is shown together with the Bragg positions as short vertical markers.

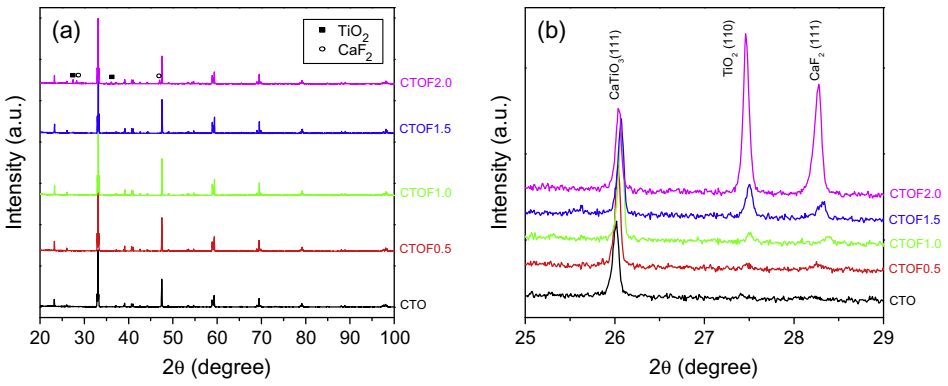

Fig. 1. (a) Powder X-ray diffraction (XRD) patterns of $CaTi(O,F)_3:Pr^{3+}$ measured in Bragg–Brentano geometry at room temperature. (b) Enlarged XRD patterns in the angular range 25–29° (2θ) indicating the presence of secondary phases.

Table 2
Rietveld refinement results of $CaTi(O,F)_3:Pr^{3+}$.

Compound	CTO	CTOF0.5	CTOF1.0	CTOF1.5	CTOF2.0
Lattice parameter (Å)					
a	5.3838(1)	5.3827(1)	5.3826(1)	5.3817(1)	5.3819(1)
b	5.4397(1)	5.4413(1)	5.4421(1)	5.4426(1)	5.4417(1)
c	7.6438(1)	7.6425(1)	7.6426(1)	7.6415(1)	7.6416(1)
Unit-cell volume (Å^3)	223.859(3)	223.840(2)	223.869(2)	223.822(2)	223.796(2)
R_p	6.64	6.56	6.37	6.36	6.52
R_{wp}	8.57	8.63	8.59	8.58	8.76
R_{exp}	5.37	5.13	5.04	5.19	5.31
χ^2	2.55	2.83	2.90	2.73	2.72

Space group symmetry: *Pbnm*.
R_p, R_{wp}, R_{exp}, and χ^2 are the reliability factors and goodness-of-fit, respectively.

deficiency as well as a reduced oxidation state of Ti or Pr by substitution of O^{2-} by F^- cannot be excluded. Typically, these defects are known to lead to unit-cell expansion [16]. Neither fluorination of $CaTiO_3$ nor generated oxygen vacancy and/or changed oxidation state of Ti alone can account for the change of lattice parameter, especially the unit cell expansion of CTOF1.0. Clearly, the resulting lattice change is a combination of several effects. To investigate the effect of different thermochemical treatments, CTOF1.5 was annealed in Ar, air and NH_3. Rietveld refinements of the corresponding XRD patterns were conducted and the results are listed in Table 3. Compared to pristine CTOF1.5, the unit-cell volume decreased with annealing. In this study, the concentrations of fluorine in the $CaTi(O,F)_3$:Pr could not be quantitatively determined, because the synthesized samples also contained unreacted CaF_2 as a minor secondary phase. Nevertheless, F^- is incorporated in the perovskite lattice and we consider that the originally highly distorted TiO_6 octahedra in $CaTiO_3:Pr^{3+}$ become much more ordered with the fluorine substitution.

Raman spectra of the materials are displayed in Fig. 3. The seven Raman modes between 200 and 800 cm^{-1} are attributed to the orthorhombic crystal structure of $CaTiO_3$ in accordance with the XRD results and literatures [17–19]. CTOF2.0 revealed additional peaks at 442 and 617 cm^{-1} which are assigned to the characteristic Raman-active E_g and A_{1g} phonons of the TiO_2 rutile phase [20,21]. This is also in good agreement with Rietveld refinement as remnant TiO_2 was estimated to be around 5 wt.% in CTOF2.0. However, the origin of the Raman bands at around 660 cm^{-1} cannot be explained. A possible origin of this Raman peak at 660 cm^{-1} could be a weak vibronic emission band of the Pr^{3+} due to the $^1D_2 \rightarrow {}^3H_4$ transition by the 632.8 nm laser radiation.

Fig. 4 illustrates the mass changes and the analysis of evolved gases during TGA–MS experiments in synthetic air. All the fluorinated $CaTiO_3$ show gradual mass loss starting at roughly 1200 °C which can be attributed to the release of fluorine as this feature was not observed for CTO. The evolved gases were analysed by mass spectrometry as shown in Fig. 4(b). The MS-signal of HF (m/z = 20) indicates the release of HF above 1200 °C. The mass loss was in the range of 0.17–0.21%. A quantification of fluorine content was not possible because the mass loss was not completed within the measured temperature range.

Table 3
Rietveld refinement results for Ar-CTOF1.5, Air-CTOF1.5 and NH_3-CTOF1.5 powders.

Material	Ar-CTOF1.5	Air-CTOF1.5	NH_3-CTOF1.5
Lattice parameter (Å)			
a	5.3811(1)	5.3808(1)	5.3815(1)
b	5.4418(1)	5.4416(1)	5.4424(1)
c	7.6404(1)	7.6401(1)	7.6411(1)
Unit-cell volume (Å^3)	223.735(2)	223.705(2)	223.793(2)
R_p	6.36	6.45	7.68
R_{wp}	8.59	8.80	10.5
R_{exp}	5.58	5.54	5.51
χ^2	2.38	2.52	3.65

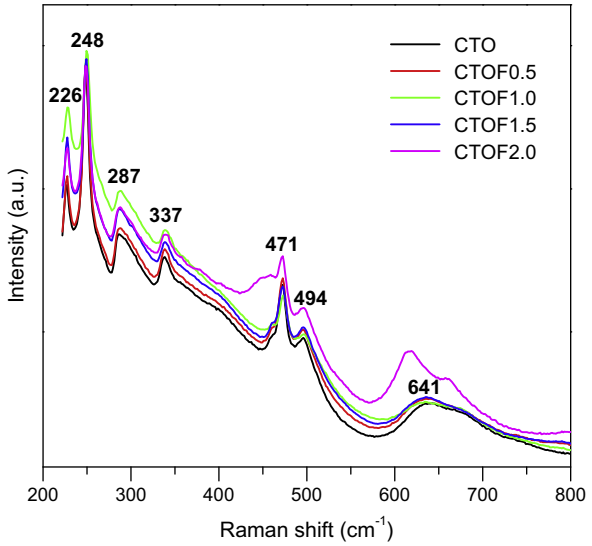

Fig. 3. Raman spectra of $CaTi(O,F)_3:Pr^{3+}$ measured at room temperature.

Fig. 5 shows the UV–Vis diffuse reflectance spectra of CTO and fluorine-substituted samples measured at room temperature. The excitation band A at roughly 330 nm is assigned to the valence-to-conduction band transition, i.e. the bandgap energy [22]. The fluorine substitution did not lead to a shift of the absorption edge, revealing that the bandgap energy of the samples was not affected as expected since the more electronegative fluorine 2*p* orbitals are located deeper in the valance band than the oxygen 2*p* orbitals. The absorption edge wavelength of roughly 330 nm is in good agreement with literature values [23]. Although the fluorine substitution did not cause a significant change in the UV region at the absorption edge, a drastic reflectance decrease was observed in the wavelength range of 355–440 nm as a shoulder B. This feature was specifically attributed to the charge transfer between Pr^{3+} and Ti^{4+} (intervalence charge transfer state, IVCT) [22,24]. And a decrease of the UV–Vis reflectance in the B band can be interpreted as decreased charge transfer between Pr^{3+} and Ti^{4+} mainly due to the $O^{2-} \rightarrow Pr^{4+}$ charge transfer [25]. In addition to the bands A and B, the reflectance spectra exhibited the characteristic 4*f*–4*f* absorption (marked as C) of the Pr^{3+} ions at 455, 476, 494 nm originating from $^3H_4$ to ^3P_J (J = 0, 1, 2) transitions [22,26] shown as an inset in Fig. 5. The UV–Vis diffuse reflectance spectra of $CaTi(O,F)_3:Pr^{3+}$ powders annealed at different atmospheres are shown in Fig. 6. A drastic decrease was observed in the wavelength range of 355–440 nm as a shoulder B for the Air-CTOF1.5. Although the annealing temperature in air was lower than the synthesis temperature, this additional heat treatment seems to oxidize the sample further. Compared to pristine CTOF1.5, it is evident that the intensity of band C is significantly increased for NH_3-

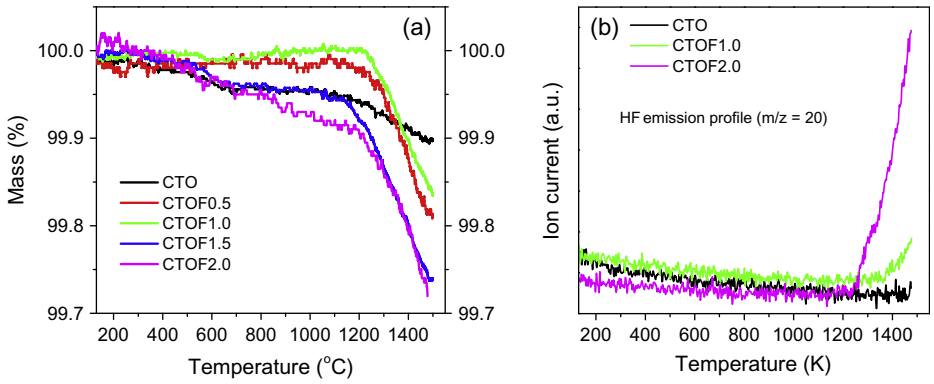

Fig. 4. (a) Thermogravimetric analysis (TGA) and (b) mass spectrometry (MS) carried out during the thermal reoxidation of $CaTi(O,F)_3$:Pr in synthetic air.

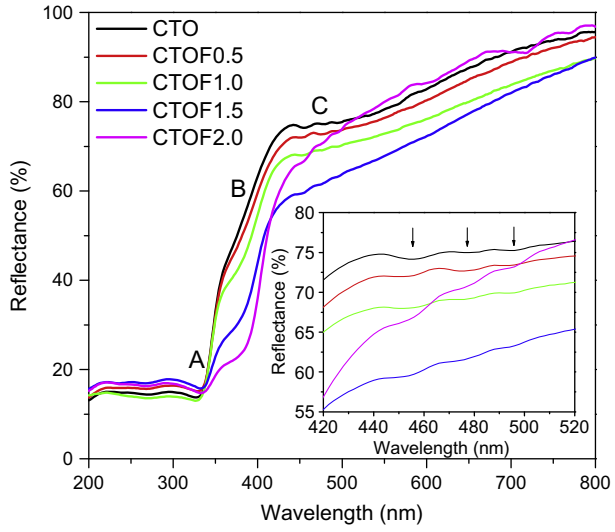

Fig. 5. UV–Vis diffuse reflectance spectra for $CaTi(O,F)_3$:Pr measured at room temperature. The inset shows the enlarged region between 420 and 520 nm.

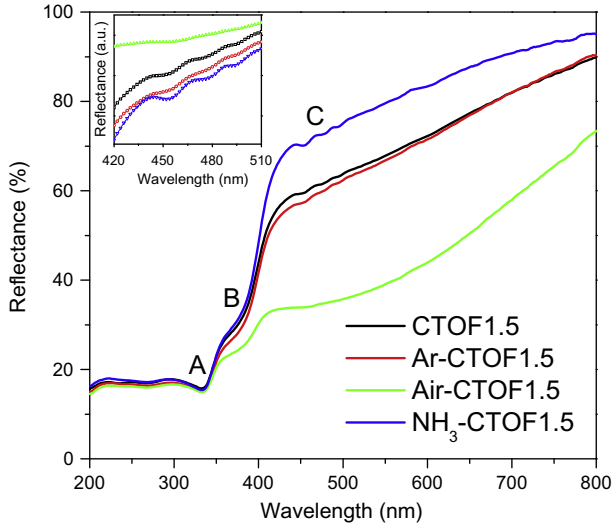

Fig. 6. UV–Vis diffuse reflectance spectra of $CaTi(O,F)_3$:Pr^{3+} annealed at different atmospheres. The inset shows the enlarged region 420–510 nm in which the spectra were shifted for better comparability.

CTOF1.5 and decreased for Air-CTOF1.5 revealing that Pr^{3+} was partly oxidized to Pr^{4+} at high temperature during the annealing in air. On the other hand, it is important to note that minor amounts of Pr^{4+} existing in the pristine CTOF1.5 was reduced to Pr^{3+} under NH_3 flow leading to distinctive features in the bands C.

Fig. 7 shows photoluminescence excitation spectra ($\lambda_{emission}$ = 611.8 nm) measured at room temperature. The band A′ at roughly 330 nm was attributed to the bandgap excitation of the $CaTiO_3$ host (the valence to conduction band transition) corresponding to the band A in the UV–Vis diffuse reflectance spectra (Fig. 6) [1,27]. CTO and CTOF2.0 powders show a peak shift to 318.4 nm. At lower energies, the band B′ at 370 nm was assigned to a charge transfer between Pr^{3+} and Ti^{4+} (corresponding to the band B in Fig. 6) [28]. The weak excitation bands C′ between 450 and 500 nm correspond to characteristic $^3H_4$ to ^3P_J (J = 0, 1, 2) transitions of Pr^{3+} (inset in Figs. 5 and 7). At higher energies (between 250 and 310 nm) the band D′ has been assigned to the lowest energy 4f to 5d excitation of Pr^{3+} [22,26]. CTO shows the highest intensity of excitation band B′ among all samples, which is in good agreement with UV–Vis diffuse reflectance spectrum as shown in Fig. 5. Selected photoluminescence emission spectra ($\lambda_{excitation}$ = 330 nm) for CTO and CTOF1.5 are shown in Fig. 7(b). None of the samples show a noticeable variation of peak position and intensity with fluorine substitution. The observed peaks match well with those of previous reports [11,29–31]. Photoluminescence excitation spectra ($\lambda_{emission}$ = 613.8 nm) of CTOF1.5 annealed at different atmospheres are shown in Fig. 8. Compared to CTOF1.5, the intensity of excitation bands C′ is increased for NH_3-CTOF1.5 and decreased for Air-CTOF1.5, which is in good agreement with UV–Vis diffuse reflectance spectra. The overall findings indicate that the concentration of Pr^{3+} and Ti^{4+} was affected by different annealing conditions. Further investigations, for example, electron paramagnetic resonance (EPR) spectroscopy are planned to investigate the substitutional influence on the afterglow properties.

Fig. 9 illustrates the phosphorescence decay profiles at room temperature. The phosphorescence intensities of fluorine-substituted powders were higher than that of CTO just after UV light irradiation. The highest phosphorescence intensity is observed for CTOF1.5 among all samples within the measurement time span. Fluorine-substituted samples, however, showed comparatively fast intensity decay above roughly 50 s compared to un-substituted CTO. The phosphorescence is known to obey an exponential decay [22,32–34]. In this study, the phosphoresce decay curves were fitted with both single exponential and double exponential decay equations and it was found that curves can be well described by the double exponential decay (Eq. (1)).

$$I(t) = A_1 \exp\left(\frac{-t}{\tau_1}\right) + A_2 \exp\left(\frac{-t}{\tau_2}\right) \quad (1)$$

where t is the time, A_1 and A_2 are pre-exponential factors, τ_1 and τ_2 are the corresponding decay times for the exponential components,

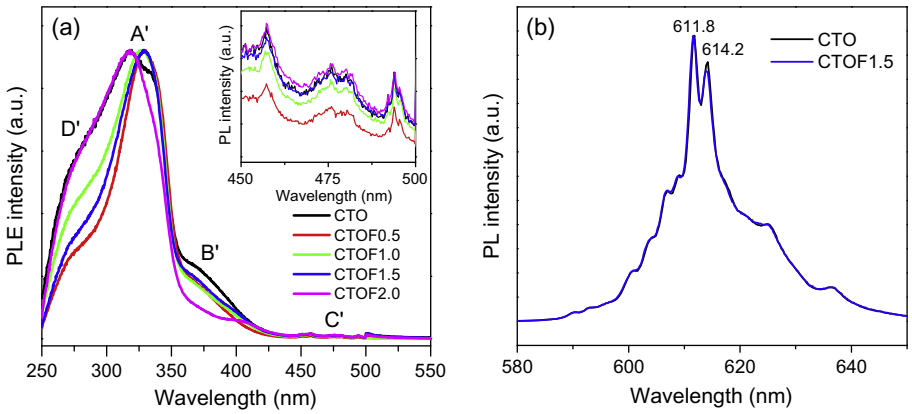

Fig. 7. (a) Photoluminescence excitation spectra ($\lambda_{emission}$ = 611.8 nm) measured at room temperature. The excitation spectra are normalized by the maximum intensity peak. (b) Photoluminescence emission spectra ($\lambda_{excitation}$ = 330 nm) of selected CTO and CTOF1.5 samples measured at room temperature.

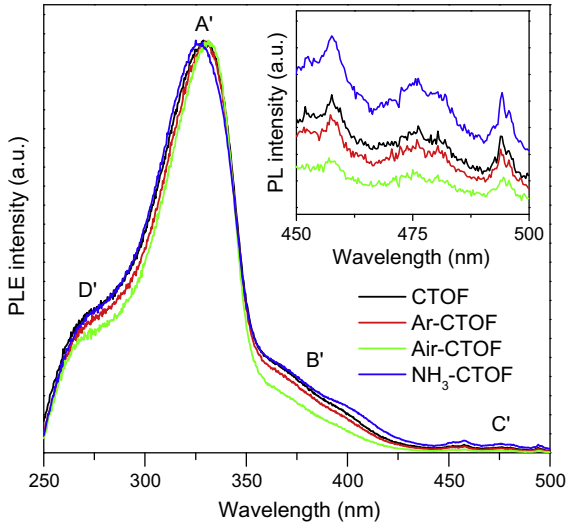

Fig. 8. Photoluminescence excitation spectra ($\lambda_{emission}$ = 613.8 nm) annealed at different atmospheres. The excitation spectra are normalized by the peak intensity at 330 nm and the inset shows the enlarged region of 450–500 nm.

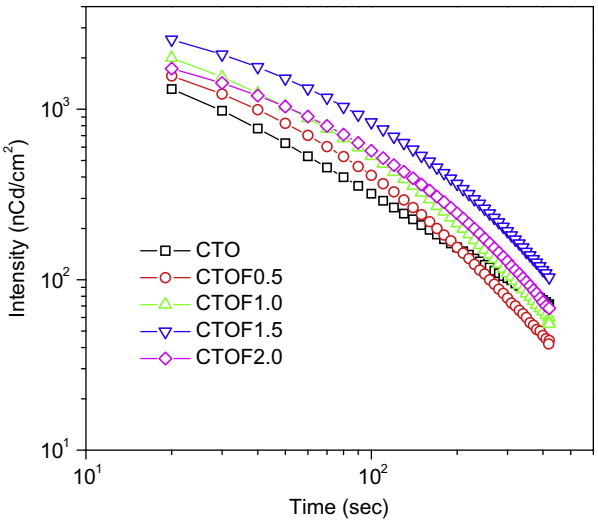

Fig. 9. Phosphorescence decay profiles for $CaTi(O,F)_3$:Pr.

respectively. The fitting results of phosphorescence decay profiles are presented in Table 4. The lifetime (τ_1) was found to be in the range of 27.7–51.5 s for all samples. Interestingly, the lifetime (τ_2)

Table 4
Fitting results of decay times τ_1 and τ_2 for $CaTi(O,F)_3$:Pr.

Compound	CTO	CTOF0.5	CTOF1.0	CTOF1.5	CTOF2.0
τ_1 (seconds)	27.7	51.5	26.9	33.4	35.0
τ_2 (seconds)	221.5	220.4	137.9	155.4	154.2

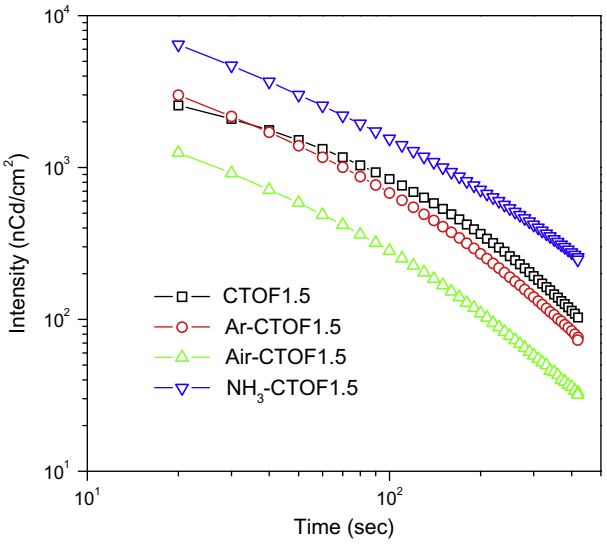

Fig. 10. Phosphorescence decay profiles of CTOF1.5 annealed in Ar, air and NH_3.

Table 5
Fitting results of decay times τ_1 and τ_2 for $CaTi(O,F)_3$:Pr annealed in Ar, air and NH_3.

Compound	Ar-CTOF1.5	Air-CTOF1.5	NH_3-CTOF1.5
τ_1 (seconds)	22.6	23.7	23.5
τ_2 (seconds)	131.1	133.2	167.1

decreased with increasing fluorine substitution, while τ_1 did not show a clear tendency. The phosphorescence decay profiles of the CTOF1.5 annealed in different atmospheres are shown in Fig. 10 and the corresponding fitting results of phosphorescence decay profiles are presented in Table 5. The phosphorescence intensity of NH_3-CTOF1.5 was by far higher than that of pristine CTOF1.5 within the measurement time span revealing an intensity improvement of ca. 450% compared to CTO. In contrast, Ar- and Air-CTOF1.5 showed reduced intensities. The lifetime (τ_1) was found to in the range of 22.6–33.4 s and interestingly, τ_2 is decreased with annealing both

in Ar and Air, but τ_2 was increased when CTOF1.5 was annealed under NH_3 reaching 167.1 s.

The luminescence properties are known to depend strongly on the defects which can be the origin of trapping and thermal detrapping of charge carriers in $CaTiO_3:Pr^{3+}$ phosphors [31,35]. In this study Pr^{3+} was added into the $CaTiO_3$ lattice as a luminescence center in addition to a partial substitution of oxygen by fluorine. It is well known that It is well known that when oxygen is substituted by fluorine, free electrons can be generated as follows in Kröger–Vink notation[36],

$$CaF_2 \overset{CaTiO_3}{\rightarrow} Ca_{Ca}^{\times} + 2F_O^{\cdot} + 2e' \quad (2)$$

Generated electrons are most probably reducing Ti^{4+} into Ti^{3+} or Pr^{4+} into Pr^{3+}. Therefore, the concentration of Pr^{3+} possibly increases with the increase of fluorine substitution, which is beneficial for the luminescence properties [37–39] explaining the enhanced luminescence intensities in this study. Annealing in moderately reducing condition (in this work, under NH_3) can be beneficial mainly in two ways. First, the influence of annealing in NH_3 can be described as regulation of the crystal structure by reducing the concentration of defects which act as non-radiative recombination centers [12] with simultaneous increase of oxygen vacancies, which are one of the most decisive factors in the increased persistent luminescence of $CaTiO_3:Pr^{3+}$. Secondly, NH_3 treatment results in reducing Pr^{4+} to Pr^{3+} which is evidently shown in the UV–Vis diffuse reflectance spectra (inset in Fig. 6) and photoluminescence excitation spectra (Fig. 8). Therefore, the concentration of Pr^{3+} was accordingly increased explaining the enhanced luminescence intensities [37–39]. In contrast, after annealing in air at 1000 °C for 12 h CTOF1.5 was oxidized, increasing the Pr^{4+} concentration and reducing the oxygen vacancies. As a result, afterglow properties are deteriorated. Hinatsu and Edelstein also reported that by using electron paramagnetic resonance (EPR), Pr^{4+} ions were identified in $BaMO_3$ and (M = Ce, Zr, Sn) and $SrCeO_3$ when the samples were kept at 1000 °C for 48 h in air [40]. Therefore, the annealing condition was found to be one of the critical factors for the improvement of photoluminescence and afterglow behavior in $CaTi(O,F)_3:Pr$ phosphors.

4. Summary

$CaTi(O,F)_3:Pr$ phosphors were successfully synthesized with different levels of fluoride substitution. All samples were characterized structurally and by thermogravimetry, and the associated luminescence properties were measured. The highest afterglow intensities were identified after NH_3-annealing, leading to an improvement of 450% versus the unsubstituted $CaTiO_3:Pr$. The improved afterglow both by fluorine substitution and by NH_3 annealing was mainly attributed to the reduction of Pr^{4+} to Pr^{3+}.

Acknowledgment

The Commission for Technology and Innovation (CTI), Swiss is gratefully acknowledged for financial support (project number, 10640.1;3 PFIW-IW).

References

[1] P.T. Diallo, P. Boutinaud, R. Mahiou, J.C. Cousseins, Phys. Status Solidi A 160 (1997) 255–263.
[2] E. Pinel, P. Boutinaud, R. Mahiou, J. Alloys Comp. 380 (2004) 225–229.
[3] X.M. Zhang, J.H. Zhang, Z.G. Nie, M.Y. Wang, X.G. Ren, X.J. Wang, Appl. Phys. Lett. 90 (2007) 151911.
[4] W.Y. Jia, W.L. Xu, I. Rivera, A. Perez, F. Fernandez, Solid State Commun. 126 (2003) 153–157.
[5] S.Y. Yin, D.H. Chen, W.J. Tang, Y.H. Yuan, J. Mater. Sci. 42 (2007) 2886–2890.
[6] J.F. Tang, X.B. Yu, L.Z. Yang, C.L. Zhou, X.D. Peng, Mater. Lett. 60 (2006) 326–329.
[7] W.J. Tang, D.H. Chen, Mater. Res. Bull. 44 (2009) 836–839.
[8] L.L. Noto, S.S. Pitale, M.A. Gusowki, J.J. Terblans, O.M. Ntwaeaborwa, H.C. Swart, Powder Technol. 237 (2013) 141–146.
[9] T. Wanjun, C. Donghua, J. Am. Ceram. Soc. 90 (2007) 3156–3159.
[10] D. Haranath, A.F. Khan, H. Chander, J. Phys. D: Appl. Phys. 39 (2006) 4956–4960.
[11] E.H. Otal, A.E. Maegli, N. Vogel-Schauble, B. Walfort, H. Hagemann, S. Yoon, A. Zeller, A. Weidenkaff, Opt. Mater. Express 2 (2012) 405–412.
[12] Songhak Yoon, Alexandra E. Maegli, Lassi Karvonen, Santhosh K. Matam, Stefan Riegg, Stefan G. Ebbinghaus, Juan C. Fallas, Hans Hagemann, Bernhard Walfort, Simone Pokrant, Anke Weidenkaff, Opt. Mater. Express 3 (2013) 248–259.
[13] P. Thompson, D.E. Cox, J.B. Hastings, J. Appl. Crystallogr. 20 (1987) 79–83.
[14] D.L. Bish, S.A. Howard, J. Appl. Crystallogr. 21 (1988) 86–91.
[15] R.D. Shannon, Acta Crystallogr. A 32 (1976) 751–767.
[16] F.J. Berry, X.L. Ren, R. Heap, P. Slater, M.F. Thomas, Solid State Commun. 134 (2005) 621–624.
[17] T. Hirata, K. Ishioka, M. Kitajima, J. Solid State Chem. 124 (1996) 353–359.
[18] H. Zheng, H. Bagshaw, G.D.C.C. de Gyorgyfalva, I.M. Reaney, R. Ubic, J. Yarwood, J. Appl. Phys. 94 (2003) 2948–2956.
[19] V.S. Marques, L.S. Cavalcante, J.C. Sczancoski, D.P. Volanti, J.W.M. Espinosa, M.R. Joya, M.R.M.C. Santos, P.S. Pizani, J.A. Varela, E. Longo, Solid State Sci. 10 (2008) 1056–1061.
[20] M. Gotic, M. Ivanda, S. Popovic, S. Music, A. Sekulic, A. Turkovic, K. Furic, J. Raman Spectrosc. 28 (1997) 555–558.
[21] H.L. Ma, J.Y. Yang, Y. Dai, Y.B. Zhang, B. Lu, G.H. Ma, Appl. Surf. Sci. 253 (2007) 7497–7500.
[22] J.C. Zhang, X.S. Wang, X. Yao, J. Alloys Comp. 498 (2010) 152–156.
[23] Y. Inaguma, T. Tsuchiya, Y. Mori, Y. Imade, N. Sato, T. Katsumata, D. Mori, Thermochim. Acta 532 (2012) 168–171.
[24] P. Boutinaud, L. Sarakha, E. Cavalli, M. Bettinelli, P. Dorenbos, R. Mahiou, J. Phys. D: Appl. Phys. 42 (2009) 045106.
[25] H.E. Hoefdraad, J. Inorg. Nucl. Chem. 37 (1975) 1917–1921.
[26] W. Jia, D. Jia, T. Rodriguez, D.R. Evans, R.S. Meltzer, W.M. Yen, J. Lumin. 119 (2006) 13–18.
[27] P.J. Deren, R. Pazik, W. Strek, P. Boutinaud, R. Mahiou, J. Alloys Comp. 451 (2008) 595–599.
[28] P. Boutinaud, E. Pinel, M. Dubois, A.P. Vink, R. Mahiou, J. Lumin. 111 (2005) 69–80.
[29] W.Y. Jia, A. Perez-Andujar, I. Rivera, J. Electrochem. Soc. 150 (2003) H161–H164.
[30] P. Boutinaud, E. Cavalli, R. Mahiou, J. Phys.: Condens. Matter 24 (2012) 295502.
[31] P. Boutinaud, E. Pinel, R. Mahiou, Opt. Mater. 30 (2008) 1033–1038.
[32] N.S. Singh, R.S. Ningthoujam, N. Yaiphaba, S.D. Singh, R.K. Vatsa, J. Appl. Phys. 105 (2009) 064303.
[33] K.S. Sohn, S.Y. Seo, H.D. Park, Electrochem. Solid-State 4 (2001) H26–H29.
[34] Y.F. Wu, Y.T. Nien, Y.J. Wang, I.G. Chen, J. Am. Ceram. Soc. 95 (2012) 1360–1366.
[35] A. Zhu, J. Wang, D. Zhao, Y. Du, Physica B 406 (2011) 2697–2702.
[36] F.A. Kröger, H.J. Vink, Relations between the concentrations of imperfections in crystalline solids, in: F. Seitz, D. Turnbull (Eds.), Solid State Physics, Academic Press, New York, 1956, pp. 307–435.
[37] X.M. Zhang, C.Y. Cao, C.H. Zhang, L. Chen, J.H. Jia, X.J. Wang, Physica B 406 (2011) 3891–3895.
[38] X.M. Zhang, C.Y. Cao, C.H. Zhang, S.Y. Xie, G.W. Xu, J.H. Zhang, X.J. Wang, Mater. Res. Bull. 45 (2010) 1832–1836.
[39] R. Fujiwara, H. Sano, M. Shimizu, M. Kuwabara, J. Lumin. 129 (2009) 231–237.
[40] Y. Hinatsu, N. Edelstein, J. Alloys Comp. 250 (1997) 400–404.